2. EXPERIMENTAL TOOLS

This chapter describes the experimental apparatus used for this analysis. This includes the Fermilab accelerator complex, a description of the detector that surrounds the collision point and many of the algorithms used to identify our γ+$\not\!\!E_T$ events. We begin with a description of the Fermilab accelerator complex, most importantly the Tevatron circular particle accelerator [48]. The Tevatron collided proton-antiproton beams at energies which were, until 2008, the most energetic collisions in the world and continued data taking in collider mode until September 2011. Surrounding one of the collision points is the experiment known as the Collider Detector at Fermilab (hereafter referred to as CDF) which recorded the energy and trajectory as well as identified the various particles produced by the proton-antiproton collisions. The various subsystems most relevant to this analysis will be described in greater detail along with details about the information they report. The readouts of these various subsystems allow us to filter out, in real time, candidate photons from the millions of collisions every second that are being produced. From this subset of events we then search for evidence of new physics by selecting candidate collisions with the signature of γ+$\not\!\!E_T$. We then use information about the arrival time of the photon and the collision time to see if any arrive delayed relative to expectations and thus possess a signature of coming from new physics. With this in mind, we turn our discussion to the Tevatron, the CDF detector, and the process by which collisions are read out of the detector in general and reconstructed in particular.

2.1 The Fermilab Tevatron

We begin by summarizing Fermilab's accelerator chain that produces a beam of protons (p) and antiprotons ($\bar{p}$) suitable for collisions in the Tevatron. The accelerator chain is described in great detail in Reference [48,49], but we give a brief overview here. Fermilab's accelerator chain is shown schematically and in aerial view in Figure

2.1. The particles begin as a hydrogen gas that is processed to make negatively ionized hydrogen with a small energy spread (keep them together in space and time) in a Cockcroft-Walton accelerator [48]. The ions are then passed to a linear accelerator (Linac) that accelerates the ions to 400 MeV and then passes them through a carbon foil in order to strip off the electrons. The protons are then passed to the next part of the accelerator known as the "booster". The booster consists of 18 Radio Frequency (RF) ferrite-tuned resonators, commonly referred to as "cavities" which accelerates the protons to 8 GeV as well as brings them closer together, commonly referred to as "bunching". During the bunching process the particles are captured into 37.7 MHz "buckets" before being passed to the next part of the accelerator known as the "Main-Injector". The Main-Injector accumulates, accelerates, and stores protons, taking them to energies of 150 GeV and combines the bunches from the booster into a single bunch. This process of bunching the protons is then repeated until a total of 36 bunches of protons have been produced. Taken together this set of 36 bunches is commonly referred to as a "train". These protons can now be passed to the final part of the accelerator chain, namely the Tevatron. In addition to providing protons to the Tevatron, the Main-Injector provides a source of protons that can be used in order to produce antiprotons. The antiprotons are created by accelerating the protons in the Main-Injector to 120 GeV and then colliding them into a target of nickel alloy. The byproduct of the collisions with the nickel target is a varied array of particles, from which antiprotons are selected and decelerated (reducing their momentum spread) in a part of the accelerator known as the "debuncher". From the debuncher the antiprotons are then passed to another accelerator system known as the "Accumulator". The Accumulator is located in the same tunnel and, as the name suggests, is where the antiprotons are accumulated and where they undergo stochastic cooling before being passed to another system known as the "Recycler". The Recycler is located in the same tunnel as the Main-Injector and uses permanent magnets to store high intensity beams of 8 GeV antiprotons. It is in the Recycler

where "electron cooling" is used to allow a more intense source of antiprotons to be produced. Electron cooling introduces a low emittance electron beam collinear to the antiproton beam and through momentum transfer the antiprotons are "cooled". The antiprotons are then bunched into 36 bunches and accelerated to 150 GeV. When this process is complete, there are 36 bunches of protons and 36 bunches of antiprotons ready to be transferred ("injected") into the Tevatron main ring to be used for high energy physics collisions [48, 49]. Within the main ring (typically just referred to as the Tevatron), which is a superconducting circular accelerator, the proton and antiproton beams are accelerated from 150 GeV to 980 GeV. The Tevatron consists of 774 superconducting dipole magnets and 240 quadrupole magnets. The former are used to bend the beam around the 3.9 mile circumference ring and the latter are used to focus the beams while electrostatic potentials accelerate the particles. The beams typically consist of $\sim 3 \times 10^{11}$ protons/bunch and $\sim 7 \times 10^{10}$ anti-protons/bunch during typical operations. These beams couter rotate in the Tevatron during data taking and are made to collide at two points along the ring, at the center of the CDF and DØ detectors as illustrated in the top of Figure 2.1. The beams remain for several hours during collisions (often referred to as a "store"). The smallest unit of data taking, referred to as a "run", is some interval of uninterrupted time during a store (or stores) where no change in detector setup or data-acquisition system has occurred. The beams collide at a center of mass energy of 1.98 TeV every 396 ns with a typical RMS in z of $\sim$28 cm, where $+z$ is defined along the direction of the proton beam, and an RMS in collision time of $\sim$1.28 ns. A basic summary of the various Tevatron parameters that existed during the data taking for this thesis, colloquially referred to as "Run II", is presented in Table 2.1. With a good understanding of the collisions, we move to the detector that surrounds the collision point, and eventually on to the algorithms that help us identify γ+$\not\!\!E_T$ events.

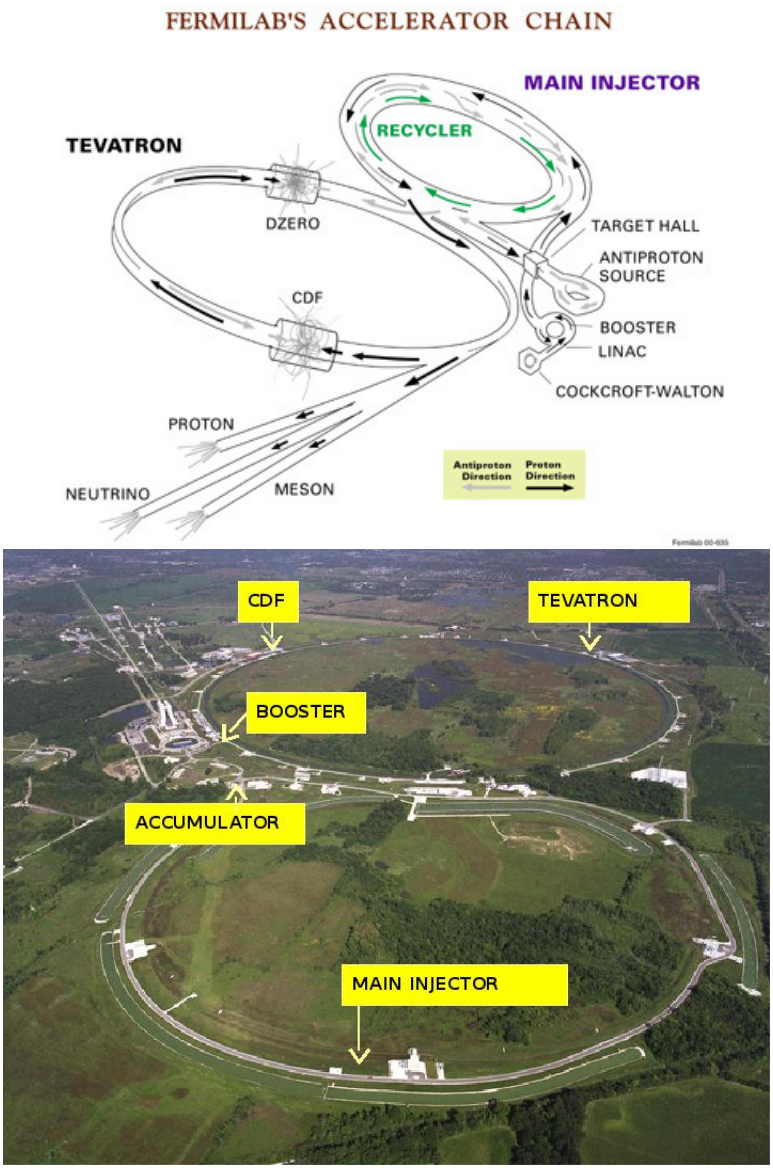

Fig. 2.1. Overview of the Tevatron accelerator complex.

2.2 The Collider Detection at Fermilab

The CDF detector is described in detail in Reference [50] and shown in Figure 2.2. We summarize here portions of the detector most relevant to this analysis. CDF is a forward-backward and cylindricaly symmetric multi-purpose detector that surrounds

Parameter (Units)	Value
Energy per Beam	980 GeV
Number of Bunches	36
Bunch Spacing	396 ns
Protons per Bunch (N_p)	$\sim 3\times10^{11}$
Antiprotons per Bunch ($N_{\bar{p}}$)	$\sim 7\times10^{10}$
Collision Point RMS in z	$\sim$28 cm
Collision Point RMS in time	$\sim$1.28 ns

Table 2.1
Summary of the Tevatron accelerator parameters during "Run II" data taking.

the collision point and is designed to identify and measure the 4-momentum of the particles produced in a $p\bar{p}$ collision. CDF makes use of a cylindrical coordinate system where the positive z axis is defined along the direction of the incoming proton beam with the origin at the center of the detector, ϕ is the azimuthal angle, and θ_0 is the polar angle relative to the z axis and defined with respect to $z = 0$ cm. Additionally, a useful angular variable, $\eta_{detector}$, known as detector pseudorapidity, that is used throughout the remainder of the thesis is defined as

$$\eta_{detector} = -ln(tan(\frac{\theta_0}{2})). \tag{2.1}$$

This variable is useful in collider physics because it describes the particles angle relative to the beam axis and the differences between two particles pseudorapidity is invariant under Lorentz boosts along the z axis. Additionally, event pseudorapidity is defined relative to the collision interaction point (event) as

$$\eta_{event} = -ln(tan(\frac{\theta_{event}}{2})). \tag{2.2}$$

where the positive z axis is defined along the direction of the incoming proton beam and θ_{event} is the polar angle is calculated from our best measured position of the

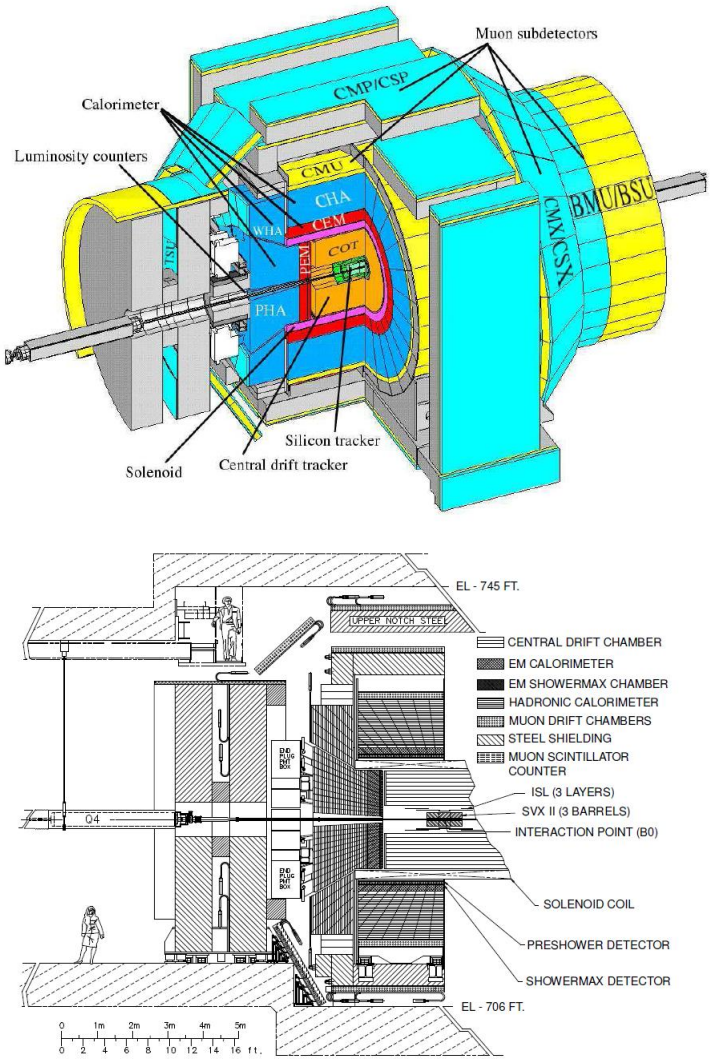

Fig. 2.2. Isometric (top) view and elevation (bottom) view of the CDF detector.

collision z. Within the central part of the CDF detector, ($|\eta_{detector}| < 1.1$), lies the main subdetectors used in this analysis. In the central region a 1.4 T magnetic field along the z direction is generated by a superconducting solenoid 1.5 meters in radius and 4.8 meters long. Within this magnetic field various tracking detectors are used to measure the trajectory of the charged particles produced during collisions. The magnetic field allows for a measurment of the sign of the charged particles, as well

as their momentum as they traverse the tracking chamber. Surrounding the tracking chambers in concentric sub-detector systems are the various energy measuring detectors, (calorimeters), and chambers used to measure and identify muons which are located outside of the solenoid and provide further particle identification and energy measurements. The combinations of the various detector components allow for the identification of particles such as photons, electrons, muons, and objects known as "jets" originating from quarks and gluons. These detectors also allow us to measure the energy and momentum of the particles and the overall imbalance of energy in the event, $\not\!\!E_T$ which is used to identify particles that leave the detector after only minimal interactions, such as neutrinos. The various identification criteria used in this analysis are described later in Section 2.4. In the following sections we characterize in greater detail the subdetectors having the most impact on this analysis. We begin with the inner most tracking detectors and work our way out radially to the calorimeters and eventually the muon chambers. After this description we will discuss how each is used as part of the reconstruction of a collision and identification of our final state particles.

2.2.1 The Tracking Systems

The part of the CDF detector closest to the beam line, as shown in Figure 2.2, is made up of a set of tracking detectors used to determine the 4-momentum and charge of charged particles passing through the various subsystems by using their measured paths and curvatures in the magnetic field. This allows us to measure the origin of the tracks in both space and time (z_0 and t_0) which are expected to come from the primary collision. Groupings of the particles' trajectories are projected back to the beam line and allow reconstruction of both the position and time of the interaction in what we refer to as the event vertex. The tracking system includes two detectors: an inner Silicon VerteX detector (SVX) and a Central Outer Tracker (COT) which surrounds it. The SVX detector is described in greater detail in Reference [51], but we

summarize the important features here. The SVX spans radially from the beam pipe from 2.5 cm$< r <$10.6 cm and covers a distance in the z-direction of 175 cm centered at the middle of the detector. The SVX consists of a silicon microstrip system used for precision position measurements which allow for 3D tracking reconstruction of trajectories. The SVX provides precision position location information for where the particles interact in the detector ("hits") that can be used in conjunction with the COT for high quality tracking as well as standalone tracking for charged particles independent of the COT at high values of $|\eta_{detector}|$. While the SVX provides a better spatial resolution on individual tracks (which is also used for vertexing), there is no timing information from the SVX system and thus it does not provide a t_0 measurement or improve upon the measurement of t_0 when it is used in conjunction with COT tracks.

The COT chamber is described in Reference [50], but we highlight the important features here. The COT surrounds the SVX system and is a cylindrical open-cell drift chamber that spans a radius of 44 cm $< r <$ 132 cm and covers a distace in z of 310 cm extending to $|\eta_{detector}| \approx$1.0. The COT is filled with a 50:50 mix of argon and ethane gas along with a small admixture of isopropyl alcohol and oxygen. This provides the COT with a maximum drift time of 100 ns (small compared to the 396 ns bunch spacing in the Tevatron). Within the COT the wires are grouped into sections of 96 layers of sense wires which are grouped into eight "superlayers" consisting of 12 wires each. As shown in Figure 2.3 the superlayers alternate between axial wires (running parallel to the beam line) and stereo wires that are tilted by 3 degrees with respect to the beam line. This allows for a high quality measurement of the kinematics of the track in the magnetic field, it's charge, as well as its initial position and time at the beam line. As charged particles pass through the chamber they ionize the gas leaving a trail of electrons which are attracted to the sensor wires by the electric field generated by the potential wires and cathodes. This allows for a determination of the time that the charged particle passed near the wire in

three dimensions with a hit resolution of 140 μm and 0.27 ns. Combining hits along the trajectory allows for the reconstruction of charged particle trajectories with a momentum resolution of $\sigma(P_T)/P_T^2 \approx 0.3\%$ (GeV/c)$^{-1}$ and a track z position at the beam line of $\sim$0.22 cm. The time information associated with each hit allows for a timing measurement of the track along the trajectory and can also be used to derive the initial time (t_0) that the particle was produced. The COT is found to have a t_0 resolution for well measured tracks to be $\sim$0.5 ns [50].

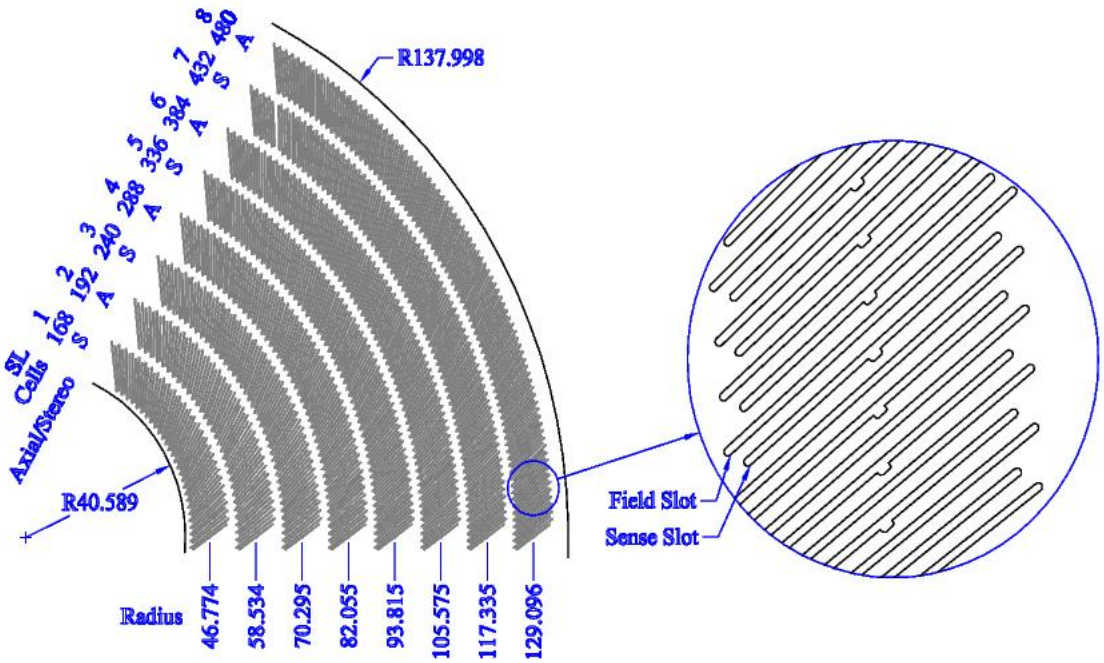

Fig. 2.3. A 1/6 section of the Central Outer Tracker (COT). The COT has eight conentric "superlayers" seperated in ϕ into "supercells", with each containing 12 sense wires between field sheets. For each "superlayer" the total number of "supercells", the wire orientation (axial or stereo), as well as the average radius is given in centimeters.

As will be discussed further in Section 2.4, the z_0 and t_0 information obtained from the combined SVX/COT is used to create verticies that are produced along the

beam line indicating where the primary collision of the proton and antiproton was likely to have occurred.

2.2.2 Electromagnetic Calorimeter

The calorimeter system at CDF is used to measure the energy and position of particles at large radii from the beam line as well as provide particle identification and a full measurement of the $\not\!\!E_T$. This becomes of particular significance when deciding which events to record from the detector based on energy measurements such as is done in this analysis. The system itself is is described in detail in Reference [50], and we provide an overview here. The calorimeters are housed just outside the solenoid and spans a radius of approximately 150 cm $< r <$ 180 cm. The calorimeter is used to measure the energy deposited by particles out to $|\eta_{detector}| < 3.64$. Since we want high quality measurements and identification of the photons in this analysis, this analysis restricts itself to only considering photons that come from the "central" ($|\eta_{detector}| < 1.0$) region. Restricting ourselves to photons in this region allows us to take advantage of the tracking having full coverage of the calorimeter and thus is the best for photon identification. The central calorimeter is constructed using a tower structure projected to the most probable collision point at the center of the detector. Each tower spans 15° in ϕ and ∼0.10 in $\eta_{detector}$, as shown in Figures 2.2 and 2.4 where all towers at the same ϕ on one side of the detector are physically grouped into what is referred to as a "wedge". Within each calorimeter tower there are two components, known as the ElectroMagnetic (EM) and the hadronic (HAD) components. During normal beam operations both the electromagnetic and hadronic calorimeter systems integrate the energy deposited in each tower of 132 ns time intervals that contain the collision time. The EM portion of a central EM calorimeter tower is known as the CEM and it lies closest to the beam line. In the CEM any interaction of an electromagnetic particle (like from a photon or electron) will deposit the overwhelming majority of its energy in this compartment. The CEM uses 23 lead

and polystyrene scintillator layers alternating in the radial direction with ∼5 mm thickness and providing 21 radiation lengths (X_0) that almost fully contain the energy cascade showers of most electromagnetic particles such as photons and electrons. Light deposited in the scintillators strips is directed out in wavelength shifting fibers to two photo multiplier tubes (PMTs) located on opposite sides of each tower which provide an energy and a timing measurement. A deposition of a large amount of energy in one or more towers of the calorimeter is commonly referred to as a "cluster". For clusters which deposit most of their energy in the EM we find a resoltuion in the CEM of $\frac{\sigma(E)}{\sqrt{E_T}} = 0.135$. At this point it is useful to define the transverse energy (E_T) as it is used throughout this thesis in different, and non-standard, ways.

- **E_T^0: Transverse Energy Relative to $z = 0$**

  The variable E_T^0 is defined as $E \cdot sin\theta_0$ where E is the energy deposited in the calorimeter and θ_0 is calculated from $z = 0$ cm at the beamline to the z position of the centroid of the energy location in the calorimeter.

- **E_T^{vtx}: Transverse Energy Relative the Highest ΣP_T Vertex**

  The variable E_T^{vtx} is defined as $E \cdot sin\theta_{vertex}$ where E is the energy deposited in the calorimeter and θ_{vertex} is calculated from z position of the highest ΣP_T vertex to the z position of the centroid of the energy location in the calorimeter. We note that the highest ΣP_T vertex is typically due to the collision that produced the energy in the detector, but this is not always the case.

A proportional strip and wire chamber, known as the Central Electron Strips (CES), is located at a depth of $\sim 6X_0$ in the CEM corresponding to the "shower maximum" for electrons and photons and is described in detail in [50]. Within each tower the CES consists of 256 cathode strips running in the ϕ direction and measure the position and profile in z with a resolution of $\sim$ 2 mm as well as 128 anode wires running in the z direction that measure the position and profile in the ϕ with a resolution of $\sim$ 2 mm in the local X coordinate. The CES is located at a radius of

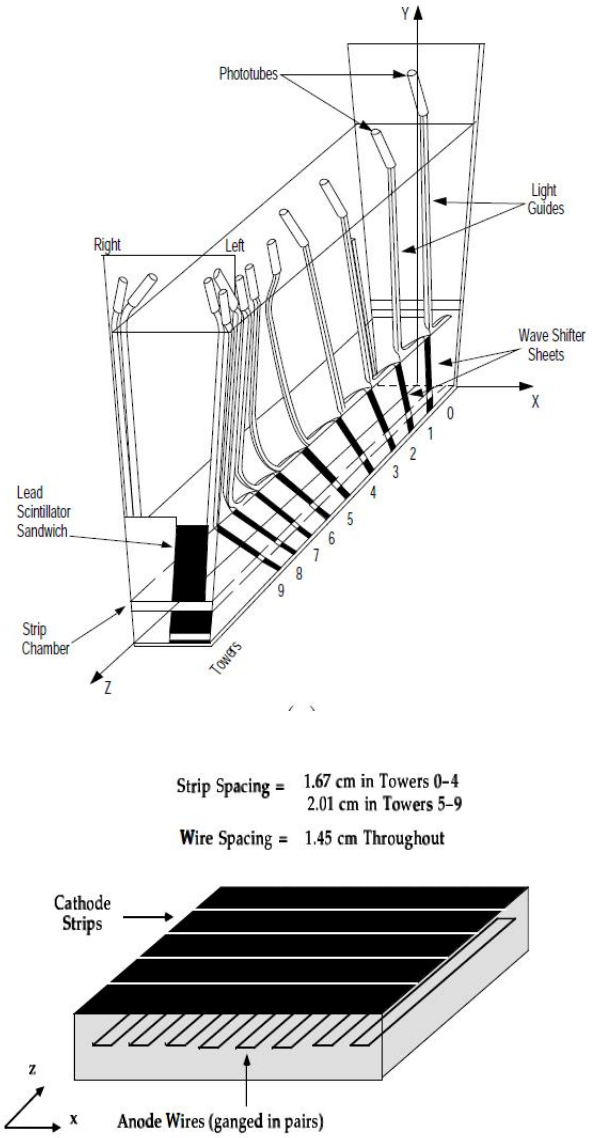

Fig. 2.4. (Top) A schematic drawing of the Central ElectroMagnetic calorimeter (CEM) including the (Bottom) Central Electron Strips (CES) sub-detector showing the strips and wires.

$\sim$ 184 cm from the beam line. The CES also provides an energy measurement with a resolution of $\frac{\sigma(E)=0.74}{\sqrt{E_T}} + 4\%$ that will be used later as well. Radially just outside the EM is the HAD calorimeter, which has the same tower-wedge geometry as the

EM but instead uses iron sampling in order to measure the energy and shower of hadronic particles. Using both the EM and Had we can identify and measure the energy of jets with an energy resolution of $\frac{\sigma(E)}{E} = 0.1E_T$ +1.0 GeV. Considering the entire calorimeter, a full measurement of the $\not\!\!E_T$ can be typically measured to a few GeV.

2.2.3 EMTiming System

One system that plays a central role in this analysis is the ElectroMagnetic calorimeter Timing system (EMTiming system) which records the time of arrival of the high energy particles particles, with $|\eta_{detector}| < 2.1$. This system is described in more detail in Reference [52] and we provide a summary of this system here. In particular it provides a measurement of t_f from Equation 1.8 and can help us separate new physics signals from SM and non-collision backgrounds. Additionally, this same handle allows us to estimate the rate at which these backgrounds contaminate our searches. This will be described in greater detail in Chapter 4, 5, and 6. Figure 2.5 shows a schematic of the signal processing that measures the arrival time using the signal from the energy in the electromagnetic shower. The EMTiming system is attached to the outputs of the PMT's which collect the scintillated light from the interaction in the calorimeter on opposite sides of each tower in the CEM and convert this energy into an analog signal. This signal is then sent to a transition board and an Amplifier-Shaper-Discriminator which converts the analog signal into a digital signal using fixed-height discriminators. This digital signal is the sent to time-to-digital converters (TDCs) for a time measurement that is then read out by the CDF data acquisition system described in Section 2.4. The EMTiming system is observed to be 100% efficient for energies above 3 GeV in the CEM with a system resolution of ∼0.5 ns [52]. The calibration and overall uniform performance of the EMTiming system is discussed in greater length in Chapter 3, but is worth noting that the system has performed with nearly 100% efficiency and negligible downtime

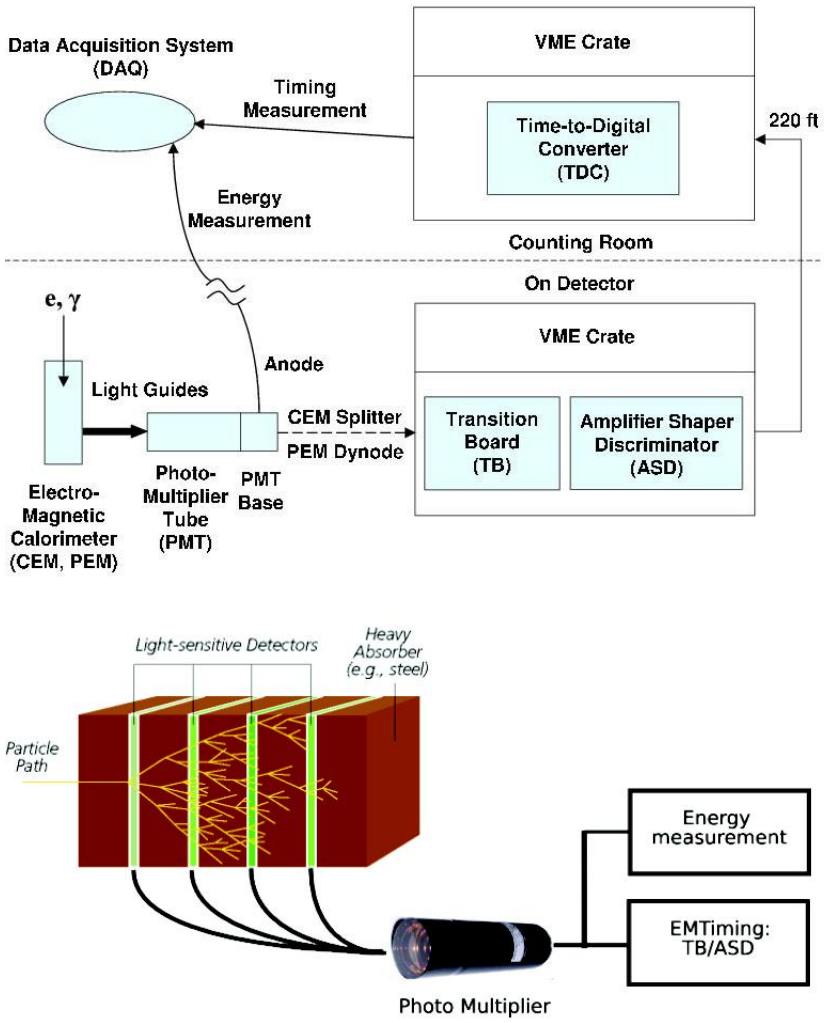

Fig. 2.5. (Top) A schematic view of the signal processing in the EMTiming system. (Bottom) A diagram demonstrating how the energy and timing measurement of a particle that showers in the calorimeter is made using the light obtained from the PMT.

since its installation and commissioning in the fall of 2004. This translates to ∼6,600 hours of of live time or over 13 million PMT-hours of successful running.

2.2.4 Muon System

Located radially behind the calorimeter is the muon identification system. The muon system is a series of 4 layer, single-wire proportional drift chambers descirbed in greater detail in Reference [53]. The muon chambers are filled with a 50-50 mix of Agron-Ethane gas at atmospheric pressure and have a drift time of $\sim 1\mu s$. The system provides a resolution of $\sim$0.6 mm in the $r-\phi$ direction and about 10 cm in the z direction with nearly 100% hit efficiency [53]. In the region $|\eta_{detector}| < 0.6$, planar drift chambers inside (CMU) and outside (CMP) the magnets return yoke are used to detect muons with P_T >1.4 GeV. Drift chambers between $0.6 < |\eta_{detector}| < 1.0$ with a conical geometry (CMX) and "Intermediate Muon Detectors" cover the region $1.0 < |\eta_{detector}| < 1.5$ for detection of muons.

When a muon passes through each layer in this system it creates a series of "hits" which can be combined using an algorithm that searches for evidence of minimum ionizing particles that travel directly through the muon chambers. Combinations of hits that are consistent with this signature are identified as a "muon-stub". For collision based-muons, if there is a track pointing to a muon-stub this is identified as a collision muon. As will be discussed later, particles coming outside the detector, such as from cosmic rays, can produce a muon stub as they traverse the muon chamber on their way to deposit energy in the EM calorimeter and be identified as a photon candidate. In this case we will find a muon-stub (with no associated track) near a photon candidate. Since the muon chambers cover most of the detector this system provides an important tool in rejecting our cosmic ray backgrounds. This special case is descibed in detail in Appendix A.

2.3 The Data Acquisition, Trigger Systems, and Good Run List

Collisions occur at the center of the CDF detector every 396 ns making the selection and storage of useful physics events while rejecting uninteresting collisions

a formidable task . The Data AcQuisition system (DAQ) at CDF, shown in Figure 2.6 and described in greater detail in Reference [54], performes this task with the necessary rejection rate of approximately 10^6:1 as only about 100 events per second can be written to record at the average logging rate of ∼23 MB/s.

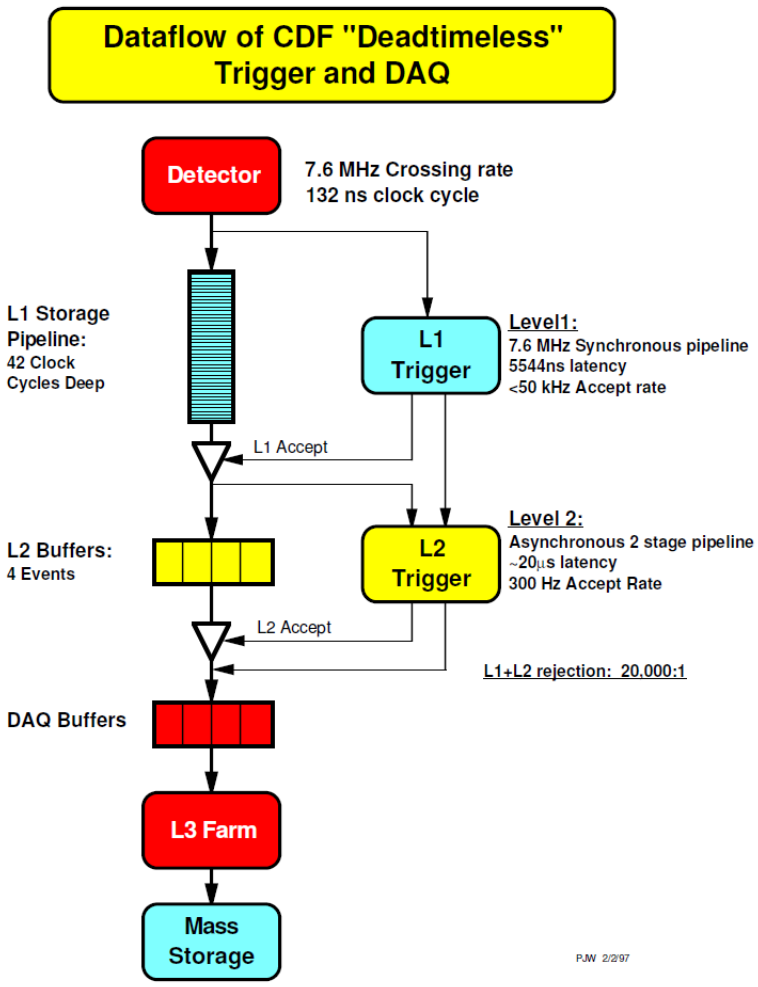

Fig. 2.6. (Top) Data flow diagram of the deadtimeless trigger and Data AcQuisition (DAQ) system at CDF [54].

To this end the CDF DAQ was built as a three-level trigger system to successively reduce the event logging rate. Each level is creatively referred to as Level 1 (L1), Level 2 (L2), and Level 3 (L3). The first two levels consist of custom built

hardware which allowes a gradual reduction of the event rate to <50 kHz at L1 and to 300 Hz at L2. Level 1 makes decisions based on simple physics quantities using a subset of information from the detector. Level 2 uses a combination of hardware and software to perform a limited event reconstruction and chooses whether or not to accept events based on calorimeter algorithms, shower information, and combined tracking information. For each event accepted by L2, the data from all the various subdetectors is combined into a single event by the Event Builder [55] and passed to L3. Level 3 consists of a farm of computers that does a full event reconstruction and selects events based on a full (albeit preliminary) set of information. L3 filters the data coming from the event builder to 100 events per second and then sends that data to be stored on computer disks. The DAQ system is designed such that there is no or minimal loss of data (no dead time). While there are many different types of events selected for readout, the events selected for this analysis are selected by a set of 3-level trigger requirements summarized in Table 2.2, and referred to as the "WNOTRACK" trigger (pronounced W no track). This selection requires a deposition of energy in the EM calorimeter (which can be seen as a very loose selection criteria for a photon candidate) and $\not\!\!E_T$ to be present in the event. As the name suggests, this trigger was originally used as a backup trigger for selecting $W \to e\nu$ events without relying on tracking measurements. We use this trigger in this analysis primarily because it is one of the only triggers available for a photon selection without the CES-χ^2 requirements. The CES-χ^2 measures the lateral shape of the energy deposition at shower maximum as measured in the CES strips and wires and compares this to test beam data using a χ^2 test. Originally designed to help reject photon pairs from π^0 decays, this requirement has been found to be inefficient for photons from long-lived particles [38]. Events passing the full set of WNOTRACK requirements are then written to permanent storage to be analyzed in greater detail later. This trigger has been found to be nearly 100% efficient [56] for electrons and photons passing our final event selection requirements.

Object Type	**Trigger**		
	Level 1	**Level 2**	**Level 3**
Electromagnetic Cluster	≥ 1 Central EM Cluster $E_T^0 > 8$ GeV $\frac{HAD(E)}{EM(E)} < 0.125$	$\lvert\eta_{detector}\rvert < 1.1$ $E_T^0 > 20$ GeV $E_T^{SeedTower} > 8$ GeV	≥ 1 EM Cluster $E_T^0 > 25$ GeV $\frac{HAD(E)}{EM(E)} < 0.125$
$\not\!\!E_T$	$\not\!\!E_T > 15$ GeV $\Sigma E_T > 1$ GeV		$\not\!\!E_T > 25$ GeV

Table 2.2
Online event selection for the WNOTRACK trigger. The variables found in this table are described in greater detail in Appendix B.

The L1 requires to have greater than 8 GeV of energy deposited in the EM-calorimeter tower used in the trigger and to have $\frac{E_{Had}}{E_{EM}} < 0.125$, in order to reject hadronic jets, as well as $\not\!\!E_T \geq 15$ GeV. L2 requires that the calorimeter clustering be central ($\eta < 1.1$) and the transverse energy $E_T > 20$ GeV. Finally, the L3 requirement for E_T and $\not\!\!E_T$ become ≥ 25 GeV.

In addition to this primary trigger, we also allow the logical *or* of a number of other associated photon triggers which all overlap with the requirements of the WNOTRACK trigger. We use these additional triggers to help ensure that we come as close as possible to 100% efficiency for selecting γ+$\not\!\!E_T$ candidate events. The summary of these other triggers can be found in Table 2.3.

Events constituting the data sample analyzed for this thesis represent data taken from approximately December 2004, when the EMTiming system was fully commissioned, to June 2010 which is about 60% of the full data taking period. In conjunction with the triggering system, a list of data taking periods for which all the necessary subsystems are functioning properly is established in what is known as a "Good Run List". In the this analysis we use a "Good Photon Run List" [57] which requires that the CEM, CES, COT, SVX, and Muon subsytems were all operational during data taking. Moreover, we apply a unique GoodEMTiming Run List that disregards

Object Type	Trigger		
	Level 1	**Level 2**	**Level 3**
ZNOTRACK			
Electromagnetic Cluster	≥ 1 Central EM Cluster $E_T^0 > 8$ GeV $\frac{HAD(E)}{EM(E)} < 0.125$	≥ 2 EM Cluster $\lvert\eta_{detector}\rvert < 1.1$ Both w/ $E_T^0 > 16$ GeV Both w/ $E_{TSeedTower}^0 > 8$ GeV	≥ 2 EM Cluster Both w/ $E_T^0 > 16$ GeV $\frac{HAD(E)}{EM(E)} < 0.125$
SUPERPHOTON70			
Electromagnetic Cluster	≥ 1 Central EM Cluster $E_T^0 > 10$ GeV	$\lvert\eta_{detector}\rvert < 1.1$ $E_T^0 > 70$ GeV $E_{TSeedTower}^0 > 8$ GeV	≥ 1 EM Cluster $E_T^0 > 70$ GeV $\frac{HAD(E)}{EM(E)} < 0.2$
PHOTON25ISO			
Electromagnetic Cluster	≥ 1 Central EM Cluster $E_T^0 > 8$ GeV $\frac{HAD(E)}{EM(E)} < 0.125$	$\lvert\eta_{detector}\rvert < 1.1$ $E_T^0 > 21$ GeV $E_{TSeedTower}^0 > 8$ GeV $E_T^{ISO} < 3$ GeV $\frac{HAD(E)}{EM(E)} < 0.125$	≥ 1 EM Cluster $E_T^0 > 25$ GeV $\text{Iso}^{Total} < 2.0$ $\chi^2 < 20$ $\frac{HAD(E)}{EM(E)} < 0.055$

Table 2.3

List of additional triggers accepted on the logical *or* of the WNOTRACK trigger. The variables found in this table are described in greater detail in Appendix B.

runs where the EMTiming system was not functioning properly (this accounts for $<$0.1 fb^{-1} reduction in luminosity). We furthermore require that all the runs within the good run lists must have an integrated luminosity ≥ 100 nb^{-1} to ensure there are sufficient statistics to calibrate over that given run period (again resulting in only a < 0.1 fb^{-1} reduction in luminosity). After these various requirements the data analyzed corresponds to an integrated luminosity of 6.3 ± 0.4 fb^{-1} as shown in Table 2.4, using the standard CDF luminosity uncertainty [58].

Period	Run Range	SAM #	$\approx$ Luminosity (pb^{-1})
1-4	190851-203799	bhelbh	460
5-10	203819-233111	bhelbi	1020
11-13	233133-246231	bhelbj	660
14-17	252836-261005	bhelbk	410
18-28	261119-289197	bhelbm	3030
29-30	289273-293800	bhelap	720
Totals	190851 - 293800		6300

Table 2.4
Table summarizing the data set used in this analysis and luminosity over the various run ranges. The SAM # is used to label the subdivision of data from the various periods. The uncertainty on the luminosity is $\sim$6% [58].

2.4 Object and Event Reconstruction

Once the events are selected from the DAQ system and written to disk they are processed "offline" where event reconstruction occurs. Offline processing consists of a series of steps to ensure the events are classified by their identified objects such as photons, electrons and $\not\!\!E_T$. The goal of this framework is to use various detectors in combination in order to reconstruct high level objects such as tracks, vertices, electrons, muons, and clusters of energy (jets). The details of how each of these objects is reconstructed is summarized in the following sections and with additional detail on some of the important identification variables given in Appendix B. From this data we select a subset of events that contain a γ+$\not\!\!E_T$.

We next describe how events are selected offline. It is useful to note that the way objects are identified in the detector will be used in many ways, for example to identify candidate events online, as well as for crude offline preselection and then later precise final selection. Indeed, many of the most sophisticated algorithms build on the simpler algorithms as their basis for selection. For example, electrons, photons and jet candidates all start by looking for clusters of energy in the calorimeter.

Photons and electrons are the subset of those clusters that are mostly in the EM calorimeter. Of the EM clusters, electrons are identified as EM clusters with a high P_T track associated with it, and photons are selected by virtue of the absense of such a track. Meanwhile the term "jet" is the catch all for clusters of energy which are neither of these, and can be due to a tau lepton, a poorly identified photon or electron, or radiation from a quark or gluon.

We begin with a general description of clusters of energy found in the calorimeter known as "jets". From this generic definition we will lay out the object identification for tracks, photons, and electrons in the CDF calorimeter and tracking chamber. Then we describe the technique to cluster together tracks at the beam line in order to identify the origin of the collision, known as the event vertex. Finally we describe the definition of $\not\!\!E_T$ by looking for imbalance of energy throughout the event in the CDF calorimeter.

2.4.1 Jets

The term "jet" in particle physics is typically used to refer to the hadronization of a high energy quark or gluon that is produced in the collision [3]. A "jet", as defined at CDF, is identified as a cluster of energy in the calorimeter. Thus, in addition to including energy deposited from quarks and gluons the term "jet" generically also includes energy deposited from the hadronic decays of taus, electrons, and photons. The algorithm to identify jets is a standard procedure used at CDF for many years and more information can be found in Reference [59]. This algorithm starts by looking at all calorimeter towers in the detector for the presence of a single tower with a large amount of energy, known as a "seed". Any single tower in the calorimeter with E_T >1 GeV may be used as a "seed" tower for looking for the presence of a jet. If there is a neighboring tower with significant energy, known as a shoulder tower, in an angular radius defined in $\eta - \phi$ space as $\Delta R = \sqrt{(\Delta\eta)^2 + (\Delta\phi)^2}$, we refer to this pair as a cluster and add up all towers within this radius; in this thesis we use a cone

of 0.4 although other analyses use 0.7 or 1.0 [59]. From this, a new energy-weighted centroid is determined and the center of the cone is re-centered there. This process is then repeated until the jet no longer changes; if two jets overlap by >50% they are merged into a single jet. Functionally, this process's primary goal is to determine the 4-momentum of the particle that produced the jet. A detailed explanation of the CDF jet calibration is beyond the scope of this thesis and can be found in reference [60]. In Table 2.5 we define the variables used to identify high E_T jets in the CDF detector using the standard jet-cone algorithm in the analysis.

Variable	Selection Requirement
E_T^0	> 15.0 GeV
$\lvert\eta_{detector}\rvert$	< 3.4

Table 2.5
Table for the standard CDF jet identifcation variables. We use a jet-cone of 0.4.

2.4.2 Tracks

As previously described, the trajectory of charged particles through the SVX and COT can be reconstructed as tracks with high quality charge, 4-momentum, and z_0 and t_0 information about when they originated at the beam line. It is this path of the charged particle that we refer to as a track. We will use tracks in three different ways in this analysis:

- **For electron and photon identification:**

  We use tracks in defining whether or not an EM cluster is from an electron or a photon. We select electron candiates if there is a high P_T track associated to an EM cluster. We select photon candidates if there is no track, or a single low P_T track, from either the SVX and COT tracking system that points to the

EM cluster. These tracks and their requirements will be described later and the variables used for selection are described in more detail in Appendix B.

- **For vertex information:**

  Tracks are used in the vertexing algorithm when attempting to reconstruct the initial time (t_0) and position (z_0) of all collisions within the event. The variables used to describe these tracks are standardized within CDF and are described in more detail in Appendix B. The requirements used to select tracks for use in the vertexing are given in Table 2.6. A detailed description of the calibration procedure for track timing is given in Chapter 3.

- **For our high P_T track veto:**

  In the final event selection, we will reject events that have a high probability of being from background events that produce a photon and $\not\!\!E_T$ in the final state, but also typically produce a high P_T track as well (e.g. $W\gamma \rightarrow l\gamma + \not\!\!E_T$ where l is a charged lepton). For this reason we will reject events with a high momentum track as part of requiring that our $\gamma+\not\!\!E_T$ events be exclusive. Events with tracks we veto have a less strict definition than ones used for timing measurement. This is because we are only looking for evidence that the final state is not exclusive $\gamma+\not\!\!E_T$ and instead contains evidence for other activity in the detector. The veto track requirements are summarized in Table 2.7.

2.4.3 Photons

Each cluster (or "jet" using the previous definition) is studied in order to determine if it is likely to have originated from a photon. The CDF detector has been used to accurately identify and measure high energy photons for over 25 years using well established identification requirements [61]. For this analysis we only consider photons found in the central part of the detector ($|\eta_{detector}| < 1.0$) owing to the fact

Variable	Selection Requirement
P_T	≥ 0.3 GeV
$\lvert\eta_{event}\rvert$	< 1.6
$COTStereoSeg(5)$	≥ 2
$COTAxialSeg(5)$	≥ 2
$\lvert z\rvert$	≤ 70 cm
$\lvert d_0\rvert$	≤ 1.0 cm
$T_0\sigma$	$0.2 < T_0\sigma < 0.8$ ns

Table 2.6

The track identification requirements used to select tracks with a good timing measurement in addition to a good position measurement for use in the SpaceTime vertexing. These variables are described in more detail in Appendix B.

Variable	Selection Requirement
P_T	≥ 10 GeV
$COTAxialSeg(5)$	≥ 2
$\frac{nCOTHits}{(LastLayerCOT+1)}$	$> 60\%$

Table 2.7

Table outlining the definition of tracks that we veto against in the exclusive $\gamma + \not\!\!E_T$ final state. These variables are described in more detail in Appendix B.

that the central region is not only better instrumented in the calorimeter and tracking chambers, but the EMTiming system has been fully calibrated and validated in this region.

The full list of photon identification requirements is given in Table 2.8 and allows us to select photons in the fiducial region of the CEM as well as being able to distinguish them from decays of $\pi^0 \to \gamma\gamma$, hadronic jets, electrons, and photon candidates from cosmic ray sources. The full description of the standard photon identification variables is given in Appendix B, but we draw attention to the fact that the list here differs slightly from the standard photon ID in five ways.

- **Eliminate CES χ^2 Variable:**

  As described before, the lateral shower shape of the photon at shower maximum as measured by the CES is normally compared to that resulting from test beam and a χ^2 fit < 20 is usually required. However, it has been shown that this is a poor selection requirement to use in searches for delayed photons which come from the decay of some long-lived heavy object [38]. This is mainly due to the fact that qualitative predictions show that the χ^2 measurement gets worse at large incident angle, but no reliable simulation is available to quantify this degradation. Thus, as was done in previous delayed photon searches, we exclude this cut.

- **PMT Aysmmetry Cut:**

  In the CEM, an energy deposit is identified from the output of the two PMTs that collect the light from the scintillator in the CEM [52], as shown in Figure 2.4. A high voltage breakdown in the PMT unrelated to an energy deposit in the CEM can create a photon candidate if this happens to occur in coincidence with a deposit of energy from a particle from a collision. We define the PMT asymmetry for a photons as:

  $$PMT_{Asymmetry} = \frac{|PMT_1 - PMT_2|}{PMT_1 + PMT_2} \tag{2.3}$$

  where PMT_1 and PMT_2 are the energy measurements as determined from each PMT individually. The total energy is determined using $\sqrt{PMT_1 \cdot PMT_2}$. As the rate of this potential background is small and the rejection power offered by the introduction of this selection requirement is nearly 100%, we simply cut away any spurious deviation from the symmetric PMT distribution expected from photons and ignore backgrounds from this source further.

- **EMTiming Requirement:**

Requiring that the EMTiming system have a reasonable readout associated with the arrival of the photon (electron) is necessary since we will use this information for calibrations. The default value in the analysis code for the EMTiming variable is set to be -999 ns and by selecting times that are less than $|900|$ ns we ensure there was a timing measurement made.

- **Additional Hadronic Energy Requriement:**

  In addition to the standard hadronic energy fraction selection requirement ($\frac{\mathrm{HAD(E)}}{\mathrm{EM(E)}}$) we have added a sliding hadronic energy selection requirement (Had(E) $\geq -0.30 + 0.008 \cdot E_T$) in order to reject against cosmic ray events. This requirement is described in more detail in Section 4.2 and Appendix B.

- **CES Energy:**

  Since we have removed the CES χ^2 requirement, we have added back a set of requirements to ensure our photon candidates are well described by a shower using the CES detector. For this reasons we use a new selection requirement of CES energy to help distinguish from high energy collision photons and photons coming from cosmic rays (CES(E)). This variable is described in greater detail in Appendix B. By requiring CES(E) >10 GeV and $\frac{\mathrm{CES(E)}}{\mathrm{TotalE}} > 0.2$ we add to our ability to reject events originating from cosmic ray events. Both these selection requirements are described in greater detail in Section 4.2 as well as Appendix B.

2.4.4 Electrons

Since electrons shower in the calorimeter in basically the same way as photons, we will use electrons throughout this thesis. We identify electron candidates as clusters of energy in the CEM in the same way as photon candidates, but with a high quality track in the COT [62]. In general we use the standard electron identification variables

Variable	Selection Requirement
$\lvert\eta_{detector}\rvert$	< 1.0 (Central)
Photon E_T^0 *(Measured from Z = 0)*	≥ 30 GeV
Fiducial (CES $\lvert X\rvert$ <21 cm, 9< CES $\lvert Z\rvert$ <230 cm)	$= 1$
$\frac{\text{HAD(E)}}{\text{EM(E)}}$	< 0.125
Energy Isolation	$E_{cal}^{iso} < 2.0 + (0.02 \cdot (E_T^0\text{-}20))$
Track Isolation	$\leq 2.0 + (0.005 \cdot E_T^0)$
N3D Track Rejection If N3D Track = 1	≤ 1 Track $P_T \leq 1.0 + (0.005 \cdot E_T^0)$
2^{nd} CES Cluster Energy	CES $E^{2nd} \leq 2.4 + (0.01 \cdot E_T^0)$
$\lvert PMTAysmmetry\rvert$	< 0.6
$\lvert EMTime\rvert$	< 900
Had (E) *Hadronic Energy deposited*	$\geq$ -0.30 + $0.008 \cdot E_T$
CES(E) *Total Energy in the CES*	$\geq$10 GeV $\frac{\text{CES(E)}}{\text{TotalE}} \geq 0.2$

Table 2.8

The identification requirements used to identify photon candidates in the γ+$\not\!\!E_T$ analysis. Note, these cuts are the standard CDF definition for photons in addition to requiring PMT Aysmmetry, EMTiming variables, total CES Energy, a sliding CES Energy fraction and additional hadronic energy requirement as well as removing CES χ^2. These variables are defined in more detail in Appendix B.

which have been used successfully at CDF for 25 years, see Reference [62], described in Table 2.9, with greater detail on electron-only variables in Appendix B, and where we have included a PMT asymmetry selection requirement and a EMTiming time requirement to make our electron and photon requirements more consistent.

The similarity between the electron clusters and the photon cluster allow us to use the electron sample as a testing place for much of our photon analysis. For example, electron candidates are used in Chapter 3 to allow us to calibrate the timing of the tracking and calorimeter systems. This is possible if we simply ignore the information

gained from the electron track and thus essentially treat the electron candidate as a photon. However, we can recover information about the origin of the electron, unlike a photon which has no track, and thus help refine various initial time and position assumptions on an event-by-event basis.

Variable	**Selection Requirement**
Electron E_T^0 *(Measured from Z = 0)*	>30 GeV
$\frac{\text{HAD(E)}}{\text{EM(E)}}$	$< 0.055 + 0.00045 \cdot \text{E}$
P_T	> 10 GeV
$\lvert\Delta Z\rvert$ CES	<5 cm
$\lvert\Delta X\rvert$ CES	<3 cm
Isolation	$< 0.1 \cdot E_T$
E/P	< 2 *(For P_T < 50 GeV)*
L_{shr}	< 2
Fiducial (CES $\lvert X\rvert$ <21 cm, 9< CES $\lvert Z\rvert$ <230 cm)	$= 1$
$\lvert Z\rvert$	< 60 cm
$\lvert PMTAysmmetry\rvert$	< 0.6
$\lvert EMTime\rvert$	< 900

Table 2.9

The identification requirements used to identify electron candidates used throughout this thesis. Note, in addition to the standard CDF variables PMT Aysmmetry and EMTiming requirements have been added to ensure a good timing measurement is made. These variables are defined in more detail in Appendix B.

2.4.5 Verticies

A typical high energy collision produces a set of tracks that all originate at the same position and time. We reconstruct a "vertex" as a grouping of tracks that originate from the beamline and collectively indicate that a paticular point in space was the origin of the tracks. In this thesis we use two different algorithms, but

begin with the main one used. The algorithm known as the SpaceTime vertexing is described in more detail in Reference [63] and this algorithm is similar to the calorimeter clustering methods. Instead of using energies in η and ϕ, it uses track P_T in, t_0 and z_0 to determine the position and time of the collision. This algorithm starts by taking the highest P_T track which becomes a "seed" of a "cluster" of tracks. Lower P_T tracks are assigned to if they lie within three standard deviations in both t_0 and z_0, where the RMS for a cluster is taken to be 0.6 ns for t_0 and 1.0 cm for z. From the remaining set of tracks, the next highest P_T track is then picked as the next seed and tracks are assigned to it, and so forth until no tracks are left. An iterative procedure does a fit of the parameters of the vertex to determine the best value of the mean and RMS of z and t_0, as well as the number of tracks in the vertex (N_{track}) and the total scalar sum of the P_T of the tracks (ΣP_T) which is a good measure of whether this vertex is due to a high q^2 collision. It then varies these parameters of all clusters simultaneously at each iteration step n, such that it maximizes the probability that all tracks belong to a set of clusters with parameters, equivalent to a likelihood fit. If, during this process, two clusters are within both 3 cm in z and 1.8 ns in t_0 the two clusters are merged. All these procedures are iterated until the variation becomes less then one percent. After the algorithm is run, we select "good" SpaceTime vertices using the requirements in Table 2.10. We note that the typical variation in z for the SpaceTime vertices is $\sim$25 cm and the variation in t_0 is $\sim$1.25 ns as discussed in more detail in Section 3.1.1.

Quantity	**Selection Requirement**
ΣP_T	$\geq$ 5 GeV
N_{track}	$\geq$ 3
$\|z\|$	$\leq$ 60 cm

Table 2.10

Table of requirements to identify good SpaceTime vertices. Tracks are required to pass the selection cuts in Table 2.6

A second vertexing algorithm which only looks for clusters of tracks in the z direction is more common at CDF and is typically referred to as the "standard vertex" algorithm. More details about it are given in Reference [64], and it has been shown to reconstruct the vertex position z with a high degree of accuracy with much better efficiency and much larger values of z along the beam line. The reason we do not use this algorithm in the main part of our analysis is that it does not separate two collisions which lie close in z but happen at a different initial times (t_0). This is a trade-off in efficiency and large z coverage for finding a vertex with a high quality measurement of the reconstructed collision time central in the calculation of t_{corr}. However, we do use this vertex algorithm to determine if events have evidence of a collision at large z since this algorithm searches for vertices out to $|z| = 150$ cm. As will be discussed in greater detail in Section 5.5.3, this becomes particularly important for minimizing highly biased events from SM sources. As summarized in Table 2.11, we search for a standard vertex with three or more tracks at $|z| >$60 cm and use this to veto events as likely having a collision at large z position, summarized in Table 2.11.

Quantity	**Selection Requirement**
N_{track}	≥ 3
$\|z\|$	> 60 cm

Table 2.11
Table of requirements to identify standard vertices which we use to veto events with evidence of activity at large collision z. This is discussed in greater detail in Section 5.5.3.

2.4.6 Missing Transverse Energy

At collider experiments, including CDF, since collisions occur with nearly no momentum in the plane transverse to the collision, we can use conservation of mo-

mentum to determine if high P_T particles left the detector. Using the fact that the vector sum of all the momenta in the final state particles should be zero in the transverse plane, particles that do not interact with the calorimeter, like the SM neutrino or the SUSY gravitino ($\tilde{G}$) will cause a momentum imbalance in the detected particles. To measure this imbalance we calculate the negative of the vector sum of all the transverse energy in the calorimeter towers with $|\eta_{detector}|$ <3.6 and refer to this as $\not\!\!E_T$. While at CDF many analyses calculate the $\not\!\!E_T$ relative to the primary collision [50], in this analysis the total deposited energy in the calorimeter is calculated relative to $z = 0$ [50]. We make this choice for reasons that will be discussed in more detail in Section 5.4, but can be understood from the fact that our dominant background is wrong vertex photons. Thus, selecting the primary vertex is not useful as it is known to be a wrong calculation. But by choosing z=0 cm we pick something equally reasonable for all events, including those with no reconstructed vertex, thus treating all events on an equal footing and using the same algorithms. Studies of minimum bias events give an estimate of the $\not\!\!E_T$ resolution of $\sim 0.4 \times \sqrt{\Sigma E_T}$, where ΣE_T is the scalar sum of the transverse energy of the towers in the calorimeter. This is typically a few GeV for the events in our final samples.

It is important to note that there are both non-collision and collision sources of $\not\!\!E_T$. As will be explored in the next sections, transverse energy will not be conserved if particles come from outside the beam or result from instrumental failure. Said differently, a photon deposited from a cosmic ray muon will create additional $\not\!\!E_T$ to the vector sum that is exactly equal and opposite to the photon candidate.

2.5 Monte Carlo Methods and Samples

Owing to the complexity of the interactions that take place in the detector during collisions, Monte Carlo (MC) simulation often provides the only way to accurately model both the background and signal processes. A complete and standardized physics process generation, detector simulation, and offline reconstruction package

is available for use with CDF analyses [66]. While these tools are expected to do a good job of reproducing many of the interactions in the detector, we do not expect them to be sophisticated enough for us to trust the true event rates of the production of the various backgrounds as a way to estimate our backgrounds. However, since they are expected to do an excellent job of reproducing the important features of interactions with the detector in general, we use these MC samples in Chapter 5 when studying the nature of the various backgrounds in the γ+$\not\!\!E_T$ final state.

The simulation begins by running an event generator, such as the PYTHIA [67] or the BAUR [68] event generators, to simulate $p\bar{p}$ collisions and then uses various theoretical cross-sections, initial and final state radiation, as well as hadronization mechanisms to simulate the decay and possible outcomes of various physics processes. The standard software package known as GEANT3 [69] is then used to simulate the interaction of these particles with the detector simulation, thus giving us detector level hit information [65]. Effects such as the additional collisions during various data taking conditions (referred to as Min-Bias events) are accounted for and added to the simulation. The output of this simulation has been shown to be an excellent approximation of the production and reconstruction of the physical processes that occur in our detector. Thus, we will be able to use this simulation as a guide for understanding possible biases which could be present in our data and potentially causing an artifical excess above background predictions. A listing of the MC samples used in this analysis is given in Table 2.12.

As the EMTiming system is not part of the standard calorimeter simulation, the arrival time for any final state particle that hits the detector is obtained using information already available in the MC simulation. Namely:

$$t_{arrival} = t_{produced} + \frac{|\vec{x}_f - \vec{x}_{produced}|}{|\vec{v}_{part}|} \tag{2.4}$$

where $\vec{v}_{part}$ is the velocity of the particle and $\vec{x}_{produced}$ is the initial position and $t_{produced}$ is the initial time [65]. The true vertex time, $t_{produced}$, takes into account

Process	**MC Stntuple**	**MC Generator**	**Luminosity** (fb^{-1})
$W \to e\nu$	`we0she, we0sge, we0sie, we0seh, we0sej`	PYTHIA	~ 11
$\gamma + jets$	`gx0s0j`	PYTHIA	~ 24
$W\gamma \to l\nu\gamma$	`re0s68` ($e\nu\gamma$) , `re0s69` ($\mu\nu\gamma$) , `re0s6a` ($\tau\nu\gamma$)	BAUR	~ 500
$W \to \mu\nu$	`we0s8m, we0s9m, we0sam, we0sbm, we0sgm`	PYTHIA	~ 7
$W \to \tau\nu$	`we0sat, we0sbt`	PYTHIA	~ 11
$Z\gamma \to \nu\nu\gamma$	`zx0s0n`	PYTHIA	$\sim 25,000$

Table 2.12
MC samples used in this analysis [65].

the simulation of the primary vertex position and time as well as the decay parent time needed to propagate through the detector volume. For photons from long-lived particles this is the neutralino decay point, for promptly produced photons, such as in $Z\gamma \to \nu\nu\gamma$, this is essentially the collision time. Since the actual data is calibrated such that the mean time of collision at the center of the detector (z= 0 cm) is set to t_0= 0 ns, the arrival time is corrected for the time of flight assuming the particle trajectory is approximately a straight line. Finally, the simulation checks to see if the particle actually interacts with the EMTiming detector and then applies a Gaussian smearing of the $t_{arrival}$ of 0.5 ns in order to model the intrinsic EMTiming resolution. This information is then recorded in the event and thus allows us to simulate the EMTiming time of MC events to compare to the data. This process has been shown to accurately reproduce the EMTiming system response and resolution to a high degree of accuracy [70].

Having firmly established the tools needed to perform the search for new physics in the exclusive $\gamma_{delayed}$+$\not\!\!E_T$ final state, we now turn our attention to the calibration and validation of the various timing systems used in this analysis.